Experimental investigation of compression properties of binary quenched Ti–Mo alloys for potential use as load-bearing implants

Article *in* MRS Advances · April 2025

DOI: 10.1557/s43580-025-01257-0

6 authors, including:

Nthabiseng Abigail Moshokoa
University of Johannesburg

Lucia Raganya
University of South Africa

Nkutwane Washington Makoana
Council for Scientific and Industrial Research, South Africa

Donald Mkhonto
Mintek

MRS Advances
https://doi.org/10.1557/s43580-025-01257-0

ORIGINAL PAPER

Experimental investigation of compression properties of binary quenched Ti–Mo alloys for potential use as load-bearing implants

N. A. Moshokoa[1] · M. L. Raganya[2] · N. W. Makoana[3] · D. Mkhonto[4] · M. J. Phasha[4] · M. E. Makhatha[1]

Received: 24 January 2025 / Accepted: 31 March 2025

Abstract

Compression properties of three binary Ti–Mo alloys for potential use as load-bearing implants were investigated in this study. Three binary alloys, namely, Ti–15Mo, Ti–17Mo, and Ti–20Mo, were designed using theoretical predictive methods and produced using a plasma melting system. Melted ingots were heat treated in a muffle furnace at 1100 °C for 1 h and quenched in ice brine water. X-ray diffraction patterns demonstrated $\beta+\alpha''$ phase peaks, deformation mechanisms showed thin parallel plates in TM15, wide deformation bands, and wavy thin lines in TM17 and wavy thin lines only in TM20 alloy. Compressive yield and ultimate strength as well as hardness decreased with an increase in Mo content. On contrary, compression strain increased with increasing Mo content.

Introduction

Due to the elderly population suffering from conditions like arthritis, the demand for prosthetic tools composed of metallic materials to replace malfunctioning hard tissues has substantially grown [1]. As human life expectancy increases, metallic biomaterials will become more and more necessary [2]. Titanium and its alloys are the most used biomaterials that are used in the production of orthopedic implants owed to a combination of properties, such as high specific strength and biocompatibility [3, 4]. An important category of Ti alloys is the metastable β type, as they possess a variety of deformation mechanisms, which depends on the stability of the β phase and extend of deformation [5, 6]. Hanada et al. demonstrated that when the β phase stability increases, several deformation mechanisms can occur, and they change in the following manner: from SIM-Twinning and then to Slip [7]. Min et al. stated that when an alloy contains mechanical twinning as the dominant deformation mechanism then high strain hardening rate and large ductility leading to lower yield strength will occur [8, 9], but when the deformation mechanism is composed of only slip then low ductility and high yield strength will occur [10]. Stress-induced martensite (SIM) in metastable β Ti alloys can result in an improved combination of strength and ductility [11].

Extensive work has been reported in controlling the β phase and the deformation mechanisms [6], although some alloy compositions have been formulated principally using the traditional trial and error method without a clear systematic fundamental basis. However, other studies have reported on the deformation mechanism in different alloys designed using the d-electron and the electron-to-atom (*e/a*) ratio methods to predict the phases present and deformation mechanism involved. Such studies include Ti–Al–Mo–V–Cr alloys reported by Sadeghpour et al. [12], Min et al. [9] in Ti–15Mo–*x*Fe alloys, and the work by Bortolan et al. [13] on Ti–Mo–Fe alloys. Despite substantial work in literature on alloys designed using the theoretical methods, the reports on systematic compression tests on the Ti–Mo binary alloys designed using theoretical methods are scarce. Thus, the current work will focus on investigating the compressive properties of quenched binary Ti–Mo alloys and their deformation mechanism predicted using theoretical methods.

✉ N. A. Moshokoa
Abigailthabi@gmail.com

1 Department of Metallurgy, University of Johannesburg, Doornfontein Campus, Johannesburg, South Africa

2 Advance Materials Engineering, CSIR, Meiring Naude Road, Brummeria, Pretoria 0184, South Africa

3 National Laser Center, CSIR, Meiring Naude Road, Brummeria, Pretoria 0184, South Africa

4 Advanced Materials Division, Mintek, 200 Malibongwe Drive, Randburg 2125, South Africa

Published online: 18 April 2025

Methodology

Theoretical predictive methods

Molybdenum equivalence (Mo_{eq}) proposed by Bania et al. was used to predict the stability of β in all the ternary alloys [14]. These predictions followed findings by Bania et al. who reported that only 10-wt.% Mo is needed to stabilize the *β* phase [14]. The equation of Moeq according to Bania is presented in Eq. 1 below. The *e/a* ratio which is a dominant factor in controlling the elastic properties and formation of phases was utilized to predict which phase the binary alloys form. Stabilization of the β phase increases as the *e/a* value is in the range 4.2–4.3 [15], 16. The calculated Moeq values are presented in Table 1, the method predicted stabilization of the β phase of all the binary alloys. The calculated *e/a* ratio indicated that TM15 and TM17 alloys will not stabilize the β phase due to the precipitated $\alpha'' + \omega$ phases, whereas TM20 alloy will retain β phase.

$$\begin{aligned}\left[Mo_{eq}\right]^{(B)} = {} & [Mo] + 0.22[Ta] + 0.28[Nb] + 0.44[W] \\ & + 0.67[V] + 1.6[Cr] + 1.11[Ni] + 2.9[Fe] \\ & + 0.77[Cu] + 1.43[Co] + 1.54Mn \\ & - 1.0[Al]\,(\%wt).\end{aligned} \quad (1)$$

The molecular orbital method was employed to give guidelines on the selection of alloying elements and also to predict the phase stability of the alloys and their deformation mechanism [4]. This approach allows theoretical determination of two electronic parameters, namely, the bond order (*Bo*), which shows the overlapping populations of the electrons between atoms and hence, a measure of the strength of the covalent bonding between atoms. As the *Bo* value increases, the stronger the chemical bond between the atoms and the metal d-orbital (*Md*) energy level correlates with the electronegativity and metallic radius of elements [17]. Phase stability map considers the general electronic parameters which are proved to be promising coordinates in designing and development of Ti alloys [4] [18].The phase stability diagram of *Bo–Md* shown in Fig. 1 presents the important information of Ti alloys, such as mechanical properties, chemical properties, and deformation mechanism. According to [19], the alloy positions in the *Bo–Md* phase stability map vary as the composition changes.

The calculated *Bo* and *Md* values are presented in Table 1 and plotted on the phase stability map in Fig. 1. The *Bo* is increased while *Md* decreases as the Mo increases, this predicts a decrease in the elastic modulus and an increase in strength. According to the phase stability map, TM15 is situated between the SIM and twin areas, TM17 is located between twin boundary and the Slip region, and TM20 is in the Slip region. The deformation mechanism is predicted to change from SIM to twining to slip with increase in Mo.

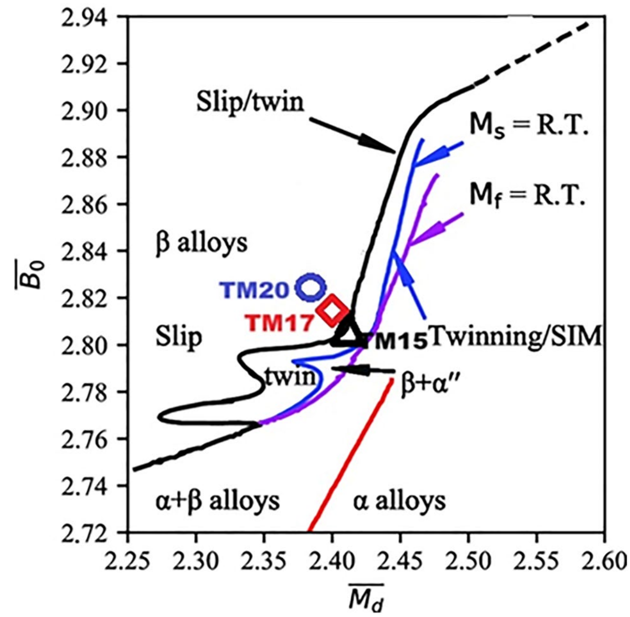

Fig. 1 Bo and Md phase stability map showing all three binary alloys under investigation [4]

Experimental procedures

Metastable β-Ti–Mo binary alloys such as TM15, TM17, & TM20 were investigated in this study. High-purity metallic powders were weighed and cold compacted into green bodies. The compacted green bodies were melted using the Ultrasonic atomization machine, AMAZEMENT re-powder Plasma melting system operated under high inert environment. The process uses an arc with a current from 70 to 270A with melting temperature 100 to 2500 °C. During melting, the compacts are placed on a copper hearth that is continuously cooled underneath with water at 17–20 °C. The cast ingots were solution treated in a muffle furnace at 1100 °C, for 1 h, and then quenched in ice brine water.

Table 1 Calculated Moeq, the *e/a* ratio, and the Bo and Md values of binary alloys

Designated name	Composition (wt.%)	Moeq (wt.%)	*e/a* ratio (at.%)	Bo	Md
TM15	Ti–15Mo	15	4.162	2.812	2.408
TM17	Ti–17Mo	17	4.185	2.815	2.402
TM20	Ti–20Mo	20	4.222	2.820	2.393

Phase analysis was executed using an X-ray diffractometer (Malvern Panalytical Empyrean Diffractometer). XRD patterns were run with Cu Kα radiation source with a secondary monochromatic source ($\lambda = 0$, 1545 nm) at 45 kV and 40 mA. OM was prepared following the metallographic preparation techniques and then etched using Kroll etchant. The OM micrographs were analyzed using the Leica Optical Microscope (OM).

Micro-Vickers hardness was measured using the Zwick Roell Vickers hardness indenter with a load of 500 gf for 10 s. Compression test samples of 3 rectangular shapes of $4 \times 4 \times 8$ per alloy were tested using the Instron^{TM} at room temperature following an ASTM standard E9.

Results and discussion

X-ray diffraction profiles

Figure 2 depicts XRD profiles of 3 investigated binary alloys. According to the XRD patterns, all the binary illustrated peaks belonging to $\beta + \alpha''$ phases. It was noticeable that the volume fraction of α'' phase decreased as the Mo content increased. This indicated that as the Mo increased, the stabilization of β phase was becoming dominant, influenced mainly by composition more than cooling rate. The presence of the α'' phase could indicate that the martensitic start temperature of the three binary alloys was above room temperature. Weak ω phase diffraction peaks were not observed in this study. This could be due to their small size and volume falling below the XRD detection limits. Thus, there is a high possibility that this phase may be present in the studied alloys; however, higher magnification analyzing techniques such as EBSD and TEM should be employed to validate its presence in these compositions.

The XRD results were comparable to the predictions of the *e/a* ratio for TM15 and TM17 alloys, because the method predicted the presence of the α″ and ω phases in addition to the β phase. However, according to the *e/a* prediction, the observed α″ martensite phase was not expected in TM20 alloy.

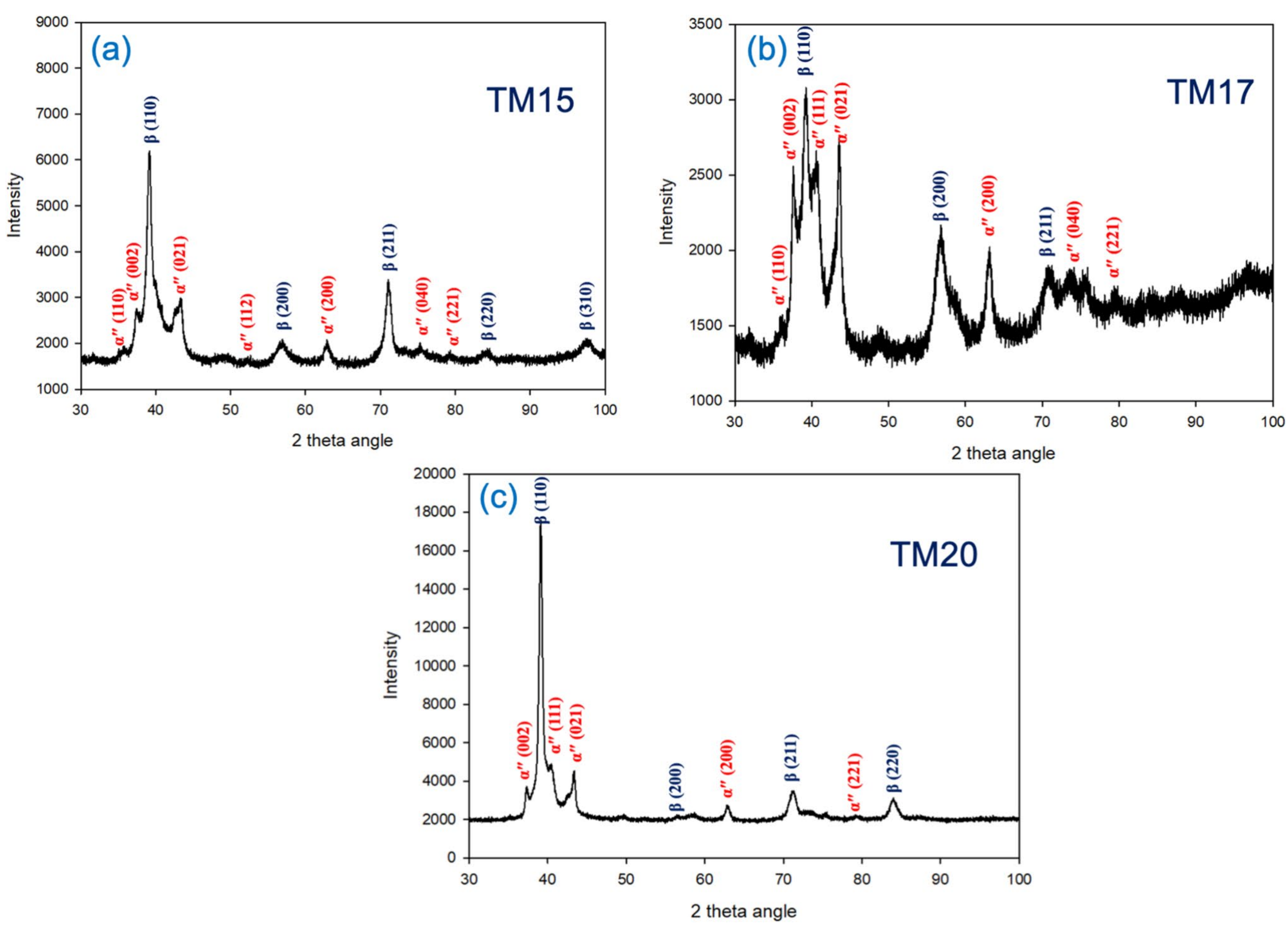

Fig. 2 X-ray diffraction patterns of water-quenched **a** TM15, **b** TM17, and **c** TM20 alloys

Optical microscope

Figure 3 illustrates light optical micrographs of binary alloys after compressive deformation. It can be observed that deformation-induced products appeared in all the alloys. Three types of deformation products can be identified as follows: thin parallel lines, wide deformation bands, and wavy thin lines. The thin parallel plates and wide deformation bands were observable in the TM15 micrograph in Fig. 3a, b. Wide deformation bands and wavy thin lines were seen in TM17 alloy in Fig. 3c, d and only wavy thin lines were demonstrated in TM20 micrographs in Fig. 3e–f. According to literature work reported by Min et al. on Ti-15Mo-xFe alloys [9] and the work of Sadeghpour et al. on Ti–Al–Mo–V–Cr-based alloys, similar deformation products were observed when characterized using the light optical microscope [12]. They reported that the thin parallel lines correspond to stress-induced martensitic (SIM), while the wide deformation modes are referred to as twins and the wavy thin lines as slip lines observed using an EBSD [5].

The deformation products of the studied alloys are similar to the light micrographs reported by the above authors. However, to validate the types of deformation mechanisms, EBSD analysis will be conducted in future work. Nonetheless, the light optical micrographs can be compared to the deformation mechanisms predicted by the *Bo–Md* phase stability map in the following way: (i) the thin parallel plated + wide deformation bands in TM15 are related to SIM and twinning deformation, (ii) the wide deformation bands and wavy slip lines in TM17are related to twinning and slip deformations, and finally (iii) the wavy slip lines in TM20 that can be correlated to the slip deformation mode.

Compression properties

Compressive yield strength, ultimate compression strength, compression strain, and micro-Vickers hardness were analyzed after conducting compression tests at room temperature. High to moderate strength in orthopedic implants is important to avoid mechanical failure. It was noticeable that the maximum compressive strength decreased from TM15 (1569 MPa), TM17 (1424 MPa) and TM20 (1308 MPa) and the yield strength decreased from TM15 (1307 MPa), TM17 (1158 MPa) and TM20 (911 MPa). Strength of a material could be affected by phases present according to the following trend: $S_{\omega} > S_{\alpha'} > S_{\alpha''} > S_{\beta} > S_{\alpha}$ [20]. TM15 and TM17 alloys with the high volume of the α″ martensitic phase and the possibility of ω phase exhibited high strength, because these phases increase the strength of a material, while the alloy with β phase only will have low strength. A similar trend was seen in the hardness values 536Hv (TM15), 405Hv (TM17) and 386Hv (TM20) which are also affected by presences of phases according to [20]. The compression strain increased slightly with an increase in Mo content (22,

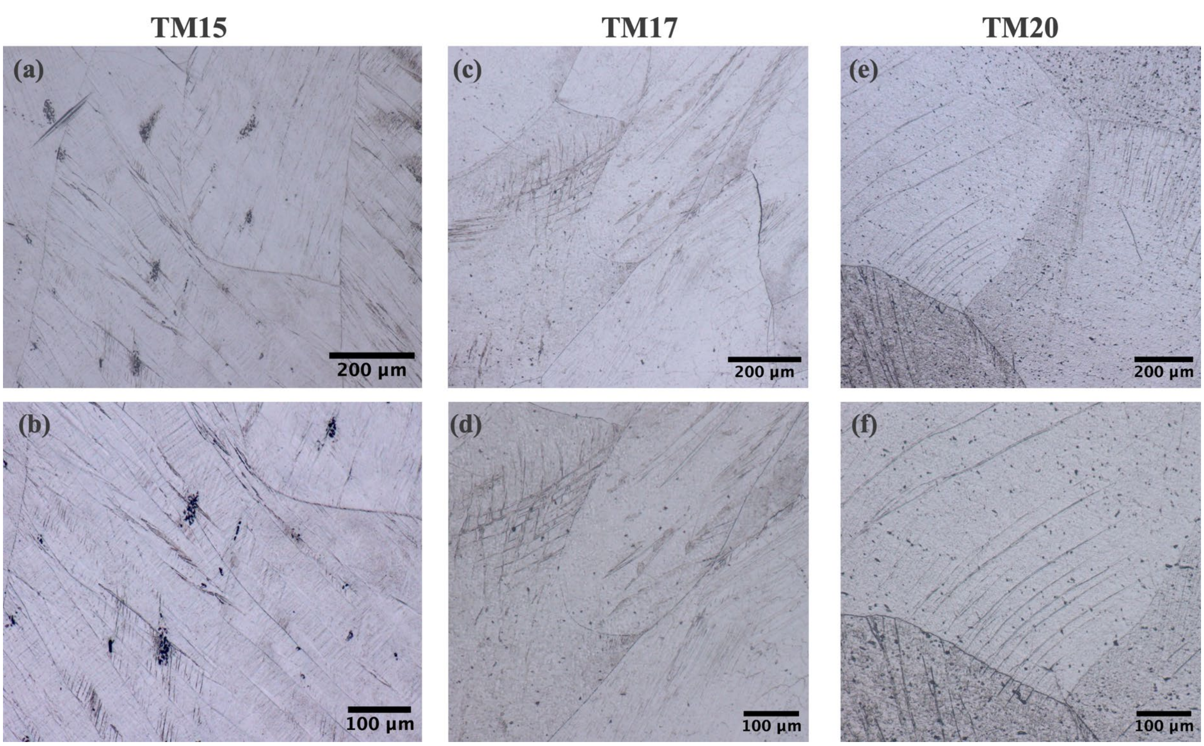

Fig. 3 Optical Microscope of water-quenched TM15 (**a** and **b**), TM17 (**c** and **d**), and TM20 (**e** and **f**) alloys

24, and 30%, respectively). The compressive yield strength of the studied alloys was found to be higher as compared to Ti–Al–Mo–V-Cr reported by Sadeghpour et al. [12].

Conclusion

This study reported for the first time the compression properties of three binary Ti–Mo alloys designed using theoretical methods for potential use as load-bearing implant materials. In general, the volume fraction of martensite phase decreased with an increase in Mo content, an indication of increased stabilization of β phase resulting to a decrease in mechanical properties. This trend also corresponded to an increase in Moeq and *e/a* ratio, promoting β phase stability. The *e/a* ratio predicted the formation of α″ and ω phases in TM15 and TM17 alloys in addition to the β phase; however, the presence of a nano-sized ω phase was too small to analyze using the XRD technique. In addition, this study observed presence of α″ martensite phase in TM20 alloy, although *e/a* ratio did not predict its existence. The deformation mechanisms upon compression tests were explained in accordance with the *Bo-Md* phase stability map. A decrease in strength and hardness is attributed to a decrease in volume fraction of hard and brittle phases. The current work paves a way of using compression properties for the development of Ti-based metastable alloys.

Acknowledgments The acknowledgment goes to Mintek (AMD) for funding the project and CSIR-IBS for funding and supporting the PhD studies.

Author contributions Nthabiseng Moshokoa contributed to conceptualization of the manuscript. Nthabiseng Moshokoa and Maje Phasha contributed to methodology. Nthabiseng Moshokoa contributed to original draft preparation: Nthabiseng Moshokoa, Maje Phasha, Washington Makoana, Lerato Raganya, Donald Mkhonto, and Elizabeth Makhatha contributed to software and resources. Moshokoa Nthabiseng and Maje Phasha contributed to validation, formal analysis, investigation, data curation, and reviewing and editing. Maje Phasha, Elizabeth Makhatha, Lerato Raganya, Donald Mkhonto, and Washington Makoana contributed to supervision. Elizabeth Makhatha and Maje Phasha contributed to funding acquisition. The funders had a role in the design of the study, collection of data, interpretation and analyses of data, editing of the manuscript, and the decision to publish the results.

Funding Open access funding provided by University of Johannesburg. We can declare that this research received no external funding.

Data availability Data will be available upon request from corresponding authors.

Declarations

Conflict of interest I Moshokoa Nthabiseng declare that there are no conflicts of interest that might influence this work.

References

1. M. Navarro, A. Michiardi, O. Castan, J. Royal Soc. Interface **27**, 1137–1158 (2008)
2. A.T. Sidambe, Mater **12**, 8168–8188 (2014)
3. Y.L. Hao, Z.B. Zhang, S.J. Li, R. Yang, Acta Mater. **60**, 2169–2177 (2012)
4. D. Kuroda, M. Niinomi, M. Morinaga, Y. Kato, T. Yashiro, Mater. Sci. Eng: A **243**, 244–249 (1998)
5. S. Hanada, O. Izumi, Meta. Trans: A **18**, 265–271 (1986)
6. E. Bertrand, P. Castany, I. Peron, T. Gloriant, Scr. Mater. **64**, 1110–1113 (2011)
7. S. Hanada, O. Izumi, Meta. Trans. A **17**, 1409–1420 (1985)
8. X.H. Min, S. Emura, T. Nishimura, K. Tsuchiya, K. Tsuzaki, Mater. Sci. Eng. A **557**, 5499–5506 (2010)
9. X.H. Min, T. Nishimura, S. Emura, N. Sekido, K. Tsuzaki, K. Tsuchiya, Mater. Sci. Eng. A **527**, 1480–1488 (2010)
10. A. Bhattacharjee, V.K. Varma, S.V. Kamat, A.K. Gogia, B.P. Kashyap, Mater. Trans. **37**, 1423–1433 (2006)
11. A.G. Paradkar, S.V. Kamat, A.K. Gogia, B.P. Kashyap, Mater. Sci. Eng. A **520**, 168–173 (2009)
12. S. Sadeghpour, S.M. Abbasi, M. Morakabati, A. Kisko, L.P. Karjalainen, D.A. Porter, J. Alloys Compd. **746**, 206–217 (2018)
13. C.C. Bortolan, L.C. Campanelli, P. Mengucci, G. Barucca, N. Giguere, N. Brodusch, C. Paternoster, C. Bolfarini, R. Gauvin, D. Mantovani, J. Alloys Compd. **925**, 166757 (2022)
14. P.J. Bania, JOM **46**, 16–19 (1994)
15. M. Tane, D. Akita, T. Nakano, K. Hagihara, Y. Umakoshi, M. Niinomi, H. Mori, H. Nakajima, Acta Mater. **58**, 6790–6798 (2010)
16. M. Ikeda, M. Ueda, R. Matsunaga, M. Ogawa, M. Niinomi, Mater. Trans. **50**, 2737–2743 (2009)
17. M. Ahmed, D. Wexler, G. Casillas, O.M. Ivasishin, E.V. Pereloma, Acta Mater. **84**, 124–135 (2015)
18. M. Abdel-Hady, H. Fuwa, K. Hinoshita, H. Kimura, Y. Shinzato, M. Morinaga, Scr. Mater. **57**, 1000–1003 (2007)
19. M. Abdel-Hady, K. Hinoshita, M. Morinaga, Scr. Mater. **55**, 477–480 (2006)
20. C. Lee, C.P. Ju, J.H. Chern Lin, J. Oral Rehabil. **29**, 214–322 (2002)